2008 IEEE International Conference on
Robotics and Automation
Pasadena, CA, USA, May 19-23, 2008

Speed and Height Control for a Special Class of Running Quadruped Robots

Nicholas Cherouvim and Evangelos Papadopoulos, *Senior Member, IEEE*

Abstract— **In this work a novel control method is presented for controlling the forward speed and apex height of a special class of running quadruped robot, with a dimensionless inertia of 1, and one actuator per leg. Seeking to minimize the parasitic pitching motion in running, pronking is used as the target gait. The control design is based on the robot dynamics, allowing its application to a wide range of robots of the class studied. Moreover, the controller adjusts the robot speed and height, requiring knowledge only of the robot physical parameters. The control ensures that negative actuator work during the stance phase is zero, thereby reducing the power expenditure. Small, off-the-shelf DC motors are adequate for the control implementation, while results of application to a detailed robot model show good performance even when including leg mass, foot collision, motor limitations, foot slipping and other factors.**

I. Introduction

Recently, the potential of using legs for efficient locomotion over varied terrain has inspired much research. Quadrupeds excite particular interest, as they are stable when stationary, unlike most two legged robots. Also, they retain simpler dynamics than robots with six legs.

There is much work on quadruped control, both in design and applications, especially using two or more actuators per robot leg. Raibert controlled a quadruped's forward speed using two actuators per leg, [1]. Using delayed feedback control a bounding gait was stabilized, though the speed could not be directly set, [2]. Fuzzy control has been applied to set the speed of a gallop [3], while CPG's have been used on the Tekken quadruped, with three actuators per leg, [4].

Although forward speed control has also been achieved using one actuator per leg, trial and error determination of controller parameters is required. The Scout II quadruped achieved stable gaits with one actuator per leg, [5], [6], with control parameters found by trial and error. Also, speed setting is reported for a walking gait, [7]. It is worth noting that most controllers are applicable to specific robots.

Using two actuators per leg rather than one simplifies control design, by adding system inputs. However, this also complicates robot design, has a severe effect on weight and cost, and increases power supply demands. So an important open issue is how to control both forward speed and attained apex height, using one actuator per leg and with no need for trial and error selection of control parameters.

In this work, this control issue is studied with the added requirement that the parasitic pitching motion, often present in quadruped running, shall be minimized. To this end, a particular design class of quadruped, described in Section II, is studied. Also, in Section III, pronking is selected as the desired gait, as it does not involve pitching. The control is designed in Section IV utilizing analytical robot dynamics. Further, no actuator negative work is present during stance, which reduces energy expenditure. Finally, in Section V, controller performance is shown for application to a robot model including all major real-world characteristics.

II. Quadruped Robot

A. Quadruped robot design and gait evolution

The quadruped robot studied has springy legs actuated at the hips, which is the only robot actuation, see Fig. 1a. This is the type of quadruped that the Scout II robot belongs to, [5], [6], which has run with a variety of gaits. A special class of this robot type is studied, for which the body inertia I, body mass m_b and half the hip spacing, d give a dimensionless inertia of $j=I/(m_b d^2)=1$. This selection is inspired by the decoupling of the vertical and pitching modes of motion, for $j=1$. Murphy found that when $j<1$, the pitching motion in running is stable, while it is unstable for $j>1$. When, $j=1$ the vertical and pitching modes are decoupled [8]. This inspires the selection of this robot class, which facilitates a decoupled approach to pitching control and avoids triggering of pitching dynamics by other DOF. A dimensionless inertia of 1 is simply achieved by proper hip placement or mass redistribution.

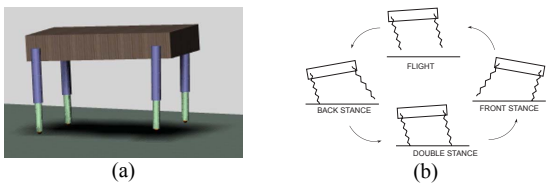

(a) (b)

Fig. 1 (a) Quadruped robot and (b) gait phases.

The gaits referred to are the pronk, in which all the robot legs are always in phase, and the bound, in which the back pair of legs is in phase, as is the front pair. The bound may involve up to four motion phases, see Fig. 1b, while the pronk has only the double stance and flight phases. Next, a simplified planar model used for control design is shown.

This work is co-funded by public funds (European Social Fund 75% and General Secretariat for Research and Technology 25%) and private funds (Zenon S.A), within measure 8.3 of Op.Pr.Comp., 3rd CSP - PENED 2003.

N. Cherouvim is with the Department of Mechanical Engineering, National Technical University of Athens, Athens, 15780, Greece. (e-mail: ndcher@mail.ntua.gr, phone: +(30) 210-772-2643).

E. Papadopoulos is with the Department of Mechanical Engineering, National Technical University of Athens, Athens, 15780, Greece (e-mail: egpapado@central.ntua.gr, phone: +(30) 210-772-1440, fax: +(30) 210-772-1455).

For the control evaluation in Section V, a second detailed model, including all major real-world properties, is used.

B. Simplified model for control design

The simplified planar model is shown in Fig. 2. The body has its center of mass (CoM) at its geometrical center, and is supported on two springy legs. The legs each have total mass m_l, inertia I_l, and are actuated by torques τ_f, τ_b at the hips. Each model leg has twice the mass, inertia and spring stiffness of a robot leg and includes viscous friction, of viscous coefficient b. Table 1 shows quantities used.

The influence of the leg mass on stance phase dynamics is negligible, and for the double stance phase a Lagrangian approach is used for the model dynamics, using body Cartesian coordinates, x, y, and pitch, θ, as generalized variables. The dynamics in terms of x, y, θ has a lengthy form, but observation shows that certain complex expressions of x, y, θ, actually represent the leg angles γ_b, γ_f, and leg lengths l_b, l_f, see Fig. 2. Substituting these expressions, the dynamics assumes a more compact form. The dynamics is shown in (1) to (3), while l_b, l_f, γ_b, γ_f are given as expressions of x, y, θ in (4) to (7).

$$\begin{aligned} &m_b\ddot{x}+k(L-l_b)\sin\gamma_b+k(L-l_f)\sin\gamma_f-b\cdot\dot{l}_b\sin\gamma_b \\ &-b\cdot\dot{l}_f\sin\gamma_f=-\tau_f\cos\gamma_f/l_f-\tau_b\cos\gamma_b/l_b \end{aligned} \tag{1}$$

$$\begin{aligned} &m_b\ddot{y}-k(L-l_b)\cos\gamma_b-k(L-l_f)\cos\gamma_f+b\cdot\dot{l}_b\cos\gamma_b \\ &+b\cdot\dot{l}_f\cos\gamma_f=-mg-\tau_b\sin\gamma_b/l_b-\tau_f\sin\gamma_f/l_f \end{aligned} \tag{2}$$

$$\begin{aligned} &I\ddot{\theta}+d\cdot k\cos(\gamma_b-\theta)(L-l_b)-d\cdot k\cos(\gamma_f-\theta)(L-l_f) \\ &-bd\cos(\gamma_b-\theta)\dot{l}_b+bd\cos(\gamma_f-\theta)\dot{l}_f= \\ &(d\sin(\gamma_b-\theta)-l_b)\tau_b/l_b-(d\sin(\gamma_f-\theta)+l_f)\tau_f/l_f \end{aligned} \tag{3}$$

$$\gamma_b=\tan^{-1}(y-d\sin\theta, x_{bt}+d\cos\theta-x) \tag{4}$$

$$\gamma_f=\tan^{-1}(y+d\sin\theta, x_{ft}-d\cos\theta-x) \tag{5}$$

$$l_b=\sqrt{(-x+x_{bt}+d\cos\theta)^2+(y-d\sin\theta)^2} \tag{6}$$

$$l_f=\sqrt{(-x+x_{ft}-d\cos\theta)^2+(y+d\sin\theta)^2} \tag{7}$$

where x_{bt} is the position of the back foot, x_{ft} is the position of the front foot during the double stance phase. The double stance dynamics above also yields the dynamics for the remaining stance phases by removing non pertinent terms.

In flight, the system CoM performs a ballistic motion. Also, the angular momentum of the system of the body and two legs, with respect to the system CoM, is conserved:

$$H_O=D_1\dot{\gamma}_b+D_2\dot{\gamma}_f+D_3\dot{\theta}=const. \tag{8}$$

where D_1, D_2, D_3 are given by:

$$\begin{aligned} D_1&=(I_l m^2+l_1^2 m_1 m(m-m_1)-l_1^2 m_l^2 m\cos(\gamma_b-\gamma_f) \\ &\quad -dl_1 m^2 m_l\sin(\gamma_b-\theta))/m^2 \\ D_2&=D_1+(l_1^2 m_l^2 m\cos(\gamma_b-\gamma_f)+dl_1 m^2 m_l\sin(\gamma_f-\theta))/m^2 \\ D_3&=I+2d^2 m_l-dl_1 m_l\sin(\gamma_b-\theta)+dl_1 m_l\sin(\gamma_f-\theta)) \end{aligned} \tag{9}$$

where l_1 is the leg CoM to hip distance.

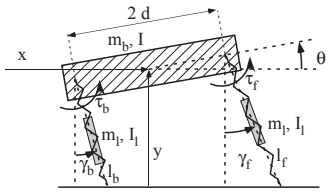

Fig. 2 Planar quadruped robot model.

TABLE 1
VARIABLES AND INDICES USED IN THE WORK

x	CoM horizontal position	L	leg rest length
y	CoM vertical position	b	viscous friction coefficient
θ	body pitch angle	g	acceleration of gravity
l	leg length	m_l	leg mass
γ	leg absolute angle	I_l	leg inertia
γ_{sum}	sum of leg absolute angles	γ_b	back leg angle
γ_{dif}	difference of leg absolute angles	γ_f	front leg angle
k	leg spring stiffness	τ	hip torque
m_b	body mass	T_{st}	stance duration
m	total robot mass	f	*as index*: front leg
I	body inertia	b	*as index*: back leg
d	hip joint to CoM distance	td	*as index*: value at touchdown

The robot motion during the double stance phase is governed by (1) to (3), and by similarly derived equations for the back and front stance phases. During flight, the CoM motion is ballistic and the pitch motion is constrained by (8).

The form of the model dynamics still remains complex for analysis due to nonlinearities and its discrete phase nature. To enable the analytical manipulation of the dynamics for the derivation of the control, certain hypotheses are made which also appear in the literature [1,12,13]. These are laid out below and referred to in the text.

Modeling hypotheses:

H1: The contribution of the dissipation forces to the stance phase forward dynamics, see (1), is negligible.

H2: To predict the change in forward speed during a stance phase, and also to compute energy dissipation due to viscous friction in the legs, the behavior of the springy legs in stance is approximated by the simple mass-spring model. The mass is equal to the robot mass, and the spring constant is equal to the sum of the robot's leg spring constants:

$$m_b\ddot{l}_b=2k(L-l_b)-mg \tag{10}$$

H3: In the stance dynamics, the leg lengths l_b, l_f are considered equal to the leg rest length L, for terms which involve the input torques τ_b, τ_f.

Gait specific hypotheses:

H4: In the pronk the back and front legs are almost parallel, so the difference between the two angles is small.

H5: For reasonable speeds, the leg angles and body pitch angle, are small enough for trigonometric small angle simplifications.

Using the above hypotheses, the dynamics is further manipulated. First, for a gait of speed $\dot{x}$, the leg angle evolution through stance is as predicted by Raibert [1]:

$$\gamma_i=\gamma_{i,td}-\dot{x}t/L \tag{11}$$

where $i=b,f$, $\gamma_{i,td}$ is the leg touchdown angle, and time t

counts from each leg touchdown. Writing the leg lengths as functions of y, θ, γ_b, γ_f, see Fig. 2, and using H3, H5, (11), the double stance dynamics in (1) to (3) becomes:

$$m_b\ddot{x}+k\cdot\gamma_b(L-l_b)+k\cdot\gamma_f(L-l_f)+\tau_b/L+\tau_f/L=0 \quad (12)$$

$$\begin{aligned} &m_b\ddot{y}+2b\cdot\dot{y}+2k\cdot y=-m_b g \\ &+2k\cdot L\cos\left((\gamma_{sum,td}/2)-(\dot{x}t/L)\right)\cos\left(\gamma_{dif,td}/2\right) \end{aligned} \quad (13)$$

$$\begin{aligned} &I\ddot{\theta}+2d^2b\cdot\dot{\theta}+2d^2k\cdot\theta=-\tau_b-\tau_f \\ &+2k\cdot L\cdot d\cdot\sin\left((\gamma_{sum,td}/2)-(\dot{x}t/L)\right)\sin\left(\gamma_{dif,td}/2\right) \end{aligned} \quad (14)$$

where $\gamma_{sum,td}=\gamma_{b,td}+\gamma_{f,td}$, and $\gamma_{dif,td}=\gamma_{b,td}-\gamma_{f,td}$. Finally, using H4, the angular momentum in (8) can be written as:

$$H_0=(I+2d^2m_l)\dot{\theta}+(I_lm^2+l_1^2m_1m(m-2m_1))(\dot{\gamma}_b+\dot{\gamma}_f)/m^2 \quad (15)$$

The simplified form of (15) may be simply integrated, and can therefore predict body pitch orientation.

To summarize, the robot model is now described by (12) to (14) during the double stance phase. During the flight phase, the CoM motion is ballistic and the pitch is constrained by (15). Below, the duration of the stance phase T_{st} is considered known, and can be found by approximately solving the vertical dynamics in (13), while neglecting friction and torque terms. Section III follows, to explain the advantages of pronking as the desired gait.

III. Pronking as the Desired Gait

The pronking gait is essentially bounding with no body pitching, and has only the flight and double stance phases. Though pronking may reduce in practice to bounding with very limited pitching, it does offer advantages in control design, as will be explained in this Section. In a two-dimensional analysis, the trotting and pronking gaits have essentially the same dynamics, while trotting is more common in nature. However, pronking was preferred in this analysis it is tranferrable in principle to the 3D problem. On the contrary, studing the trotting gait in a two dimensional analysis does not provide a solution to the 3D problem.

To begin with, the robot leg touchdown angles $\gamma_{b,td}$, $\gamma_{f,td}$, are known to be important inputs in any gait and are easily set by leg positioning during flight, so they are often used in control [1,3,5,6,12]. One issue that arises is identifying the *discreet* influence of the back and front leg touchdown angles on the dynamics, as they appear in coupled forms in the general case. For the special case of pronking it will be shown that the sum and difference of the touchdown angles, $\gamma_{sum,td}$, $\gamma_{dif,td}$, may be distinctly associated with the vertical and pitching motion modes.

First, if $\gamma_{dif,td}$ is zero as in ideal pronking, then (13) shows the vertical motion to be dependant on the sum of the touchdown angles, $\gamma_{sum,td}$. Also, for motions close to pronking, it can be seen from (14) that $\gamma_{dif,td}$ has the stronger influence on the pitching motion, as small deviations of its value from zero determine the existence of the whole term it belongs to. The distinct effect of the inputs $\gamma_{sum,td}$, $\gamma_{dif,td}$ in pronking is apparent, and this decoupling behavior facilitates the control approach in Section IV, where the motion modes are studied individually.

IV. Control Design

The control inputs to the robot system are the sum and difference of the leg angles at touchdown, $\gamma_{sum,td}$, $\gamma_{dif,td}$, and the actuator torque applied during the stance phase. The inputs $\gamma_{sum,td}$, $\gamma_{dif,td}$ are not directly controlled in the physical robot, but are fed to the actuator controllers that servo the legs to the desired touchdown positions in flight. For control design purposes the actuator torques during stance are chosen to be constant for the duration of the phase, and to be equal at the back and front hips:

$$\tau_b=\tau_f=\tau=const.\ (in\ stance) \quad (16)$$

Therefore, the three control inputs to the robot system are the leg angle inputs, $\gamma_{sum,td}$, $\gamma_{dif,td}$, and the constant torque, τ, applied in stance. The robot dynamics used for the control derivation is that presented in Section II, in (12) to (15), with generalized variables x, y, θ.

The aim in this Section is to compute the control inputs $\gamma_{sum,td}$, $\gamma_{dif,td}$, τ, given the state of the robot at liftoff from the ground. Once the inputs are computed, the hip actuators position the legs in flight. Then, at touchdown, the actuators apply a torque defined by the control input τ.

In the first three parts of this Section, each of the forward, vertical and pitching modes of motion is studied. From the study of each motion mode, a single control design equation involving the control inputs is derived. The fourth part of the Section explains how the three control design equations lead to the computation of the three control inputs.

Details of the robot feedback are given in subsection E. Here, it is relevant to say that leg lengths, leg angles, and the body pitch are measured, and the rates of change are also known. From this data, the robot state at liftoff is known, using robot geometry. An example is to compute $\dot{x}$ at liftoff for the case where the back leg lifts off last, see Fig. 2:

$$\dot{x}_{lo}=-\dot{l}_{b,lo}\sin\gamma_{b,lo}-l_{b,lo}\dot{\gamma}_{b,lo}\cos\gamma_{b,lo}-d\dot{\theta}_{lo}\sin\theta_{lo} \quad (17)$$

A. Forward motion mode

The forward motion is studied for the pronking gait with the desired forward speed $\dot{x}_{des}$. A constraint on the control inputs must be derived that ensures that the robot forward speed is the desired. In Section II, the forward dynamics are given in (12). Using (16) and H4 in (12) provides:

$$m_b\ddot{x}+2k\cdot\gamma_b(L-l_b)+2\tau/L=0 \quad (18)$$

Due to H4, the sum of the touchdown angles $\gamma_{sum,td}$ in the pronking gait is equal to twice one of $\gamma_{b,td}$, $\gamma_{f,td}$. Also, utilizing H6, and integrating (18) once, the forward speed $\dot{x}_{i+1}$ after stance can be computed, given the speed before stance, $\dot{x}_i$, as a function of the control inputs $\gamma_{sum,td}$, τ:

$$\dot{x}_{i+1}=-k\int_0^{T_{st}}(\gamma_{sum,td}-2\dot{x}_{des}t/L)(L-l_b)dt\Big/m_b-2\tau T_{st}L/m_b+\dot{x}_i \quad (19)$$

In (19), the first term on the right represents the effect of the leg spring forces on the speed, while the second term describes the effect of the hip torques. The value of the control input $\gamma_{sum,td}$ is now considered as the sum of a

nominal value plus some bias, $\gamma_{sum,td,bias}$:

$$\gamma_{sum,td} = (\dot{x}_{des} T_{st} / L) + \gamma_{sum,td,bias} \quad (20)$$

The bias $\gamma_{sum,td,bias}$ can be found by using (20) in (19), and observing the symmetry of the leg evolutions during stance, as predicted by (10). We then obtain:

$$\gamma_{sum,td,bias} = -4 \cdot \tau \cdot T_{st} \Big/ \left(m_b L(-2\dot{l}_{b,td} + gT_{st}) \right) \quad (21)$$

where $\dot{l}_{b,td}$ is the leg compression rate just after touchdown. By integrating flight dynamics, it is possible to express $\dot{l}_{b,td}$ as a function of the control input $\gamma_{sum,td}$. Therefore:

$$\dot{l}_{b,td} = f(\gamma_{sum,td}) \quad (22)$$

We have observed, when applying the control, that substituting the desired forward speed in (20) with the actual speed of the robot, $\dot{x}$, attracts the robot to the desired speed. A similar observation is made in [1], which inspired us here.

Equation (20) is the *first control design equation*. Observing (21), (22), shows the control design equation to be a constraint between the two control inputs $\gamma_{sum,td}$, τ.

B. Vertical motion mode

The apex height during flight is controlled indirectly. The quantity directly controlled is the amount of energy added during stance, via the hip torques. This results in a control on the apex height, as will be explained. To this end, consider the body energy at the flight apex:

$$E_{ap} = (m_b \dot{x}^2 / 2) + m_b g \cdot y + (I \cdot \dot{\theta}^2 / 2) \quad (23)$$

If the forward speed is controlled to the desired value and the pitching to zero, as in pronking, then from (23) the apex height is controlled by regulating the energy. So, since the controllable quantity is the energy inserted in each stance, it is sought to show that inserting the same pre-calculated energy, in every stance, controls the body's energy.

This is indeed the case if the losses of energy for a desired pronking gait can be calculated, and an amount of energy equal to these losses is inserted in each stance. Then, if the robot has a higher energy than that of the desired gait, it will have a greater apex height for the same controlled speed. Hence the losses due to the leg viscous friction will surpass the compensated pre-calculated energy losses, and the system energy decreases. In the opposite case, the apex height will increase, till it stabilizes at the desired level.

Now the energy losses for the desired pronking gait remain to be calculated so as to achieve the desired apex height, as explained above. The body energy losses, E_l, in one cycle, are due to three causes, firstly the leg viscous friction during stance, secondly the leg positioning in flight and thirdly the acceleration of unsprung leg mass at liftoff. Combining these, the body energy losses are expressed as:

$$E_l = 2b \int_0^{T_{st}} \dot{l}_b^2 dt - m(\dot{x}_{td}^2 - \dot{x}_{lo}^2)/2 - m((\dot{y}_{lo}^+)^2 - (\dot{y}_{lo}^-)^2)/2 \quad (24)$$

where $\dot{y}_{lo}^-$, $\dot{y}_{lo}^+$ indicate vertical velocities just before and just after liftoff. The three terms in (24) correspond to the three causes of energy loss described above. Given the state of the robot at liftoff, the last two terms are computable, using (17), and solving flight dynamics. The first term of (24) is computed using (10), and will be a function of the control input $\gamma_{sum,td}$ because of (22). Therefore, the body energy losses E_l for the next stance phase are a direct function of the input $\gamma_{sum,td}$, given the robot state at liftoff.

For the system energy to remain at the correct level, the losses E_l must equal the energy inserted by the actuators:

$$E_l = \int_0^{T_{st}} \tau_b (\dot{\gamma}_b - \dot{\theta}) \; dt + \int_0^{T_{st}} \tau_f (\dot{\gamma}_f - \dot{\theta}) \; dt \quad (25)$$

So, using H5, H6 and (16), in (25), it is:

$$\tau = (E_l \cdot L) / 2\dot{x} \cdot T_{st} \quad (26)$$

Using the current speed $\dot{x}$ in (26), as opposed to the desired value, ensures that the correct energy is inserted in any transient case. Equation (26) is the *second control design equation*. Note that, as explained after (24), E_l is a function of the control input $\gamma_{sum,td}$. Therefore, given the known robot state at liftoff, the second control design equation is a constraint between the control inputs $\gamma_{sum,td}$, τ. This was also the case in the first control design equation in (20), so there is now a system of two design equations with the two unknown inputs $\gamma_{sum,td}$, τ. The solution process is described in part four of this section.

C. Pitching motion mode

The third control input $\gamma_{dif,td}$ now remains to be determined. To remain close to the pronking desired gait, it is necessary to eliminate deviations of the body pitching velocity from zero. To do this, the evolution of the pitching motion is first mapped from the current liftoff of flight phase *i* through to the touchdown of flight phase *i+1*, as a function of the control inputs $\gamma_{sum,td}$, $\gamma_{dif,td}$, τ, see Fig. 3.

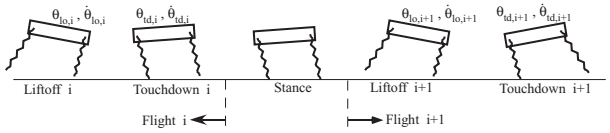

Fig. 3 Sequence of events for deriving the pitching map.

The control inputs $\gamma_{sum,td}$, τ are known from above, so the single free parameter to influence pitching is the difference of the leg touchdown angles $\gamma_{dif,td}$. The map is comprised of three parts, the first through flight *i*, the second through stance and the third through flight *i+1*. For the two flight parts, the map is given by (15), while during stance it is given by the double stance vertical and pitching dynamics in (13), (14), and the back and front stance dynamics which may be similarly derived. Using this dynamics, the vector $\mathbf{u} = [y, \theta, \dot{y}, \dot{\theta}]^T$ is mapped from liftoff of flight *i* to touchdown of flight *i+1*. The vertical motion is controlled independently in part B of this Section. Therefore, the control of pitching is implemented by computing input $\gamma_{dif,td}$, such that zero pitch velocity is obtained at the touchdown of flight *i+1*, given $\mathbf{u}$ at liftoff of flight *i*:

$$\mathbf{S} \cdot \mathbf{u_{i+1,td}} = \mathbf{S} \cdot \mathbf{f}(\mathbf{u_{i,lo}}, \gamma_{dif,td}) = \dot{\theta}_{td,i+1,des} \quad (27)$$

where $\dot{\theta}_{td,i+1,des}$ is the desired pitch velocity at touchdown, set equal to zero, see Fig. 3, and the vector $\mathbf{S} = [0,0,0,1]$

selects the pitch velocity component of **u**, and **f** represents the pitching map described above. The solution process is numerical, but is fast, as it does not involve dynamics integration, due to the analytically integrable form of stance dynamics when $I = m_b d^2$. A solution on a typical PC takes 10ms or so, which is acceptable as it is required only once per flight. Equation (27) is the *third control design equation*.

D. Computation of control inputs

Now, all three control inputs, $\gamma_{sum,td}$, $\gamma_{dif,td}$, τ, can be computed. The sum of the leg touchdown angles, $\gamma_{sum,td}$, and the torque to be applied at each hip during stance, τ, are found first by combining the first two control design equations in (20) and (26). The solution is analytical, but lengthy, and does not offer further insight into the motion. The solution process requires expanding harmonic functions of $\gamma_{sum,td}$ in a second-order Taylor series around the value $(\dot{x}_{des} T_{st} / L)$. Finally, the third control input, the difference of the leg touchdown angles, $\gamma_{dif,td}$, is found from (27).

E. Sensory feedback and control application

The sensors required for control are encoders for measuring leg angles and lengths, an inclinometer, and a rate gyro for pitch velocity and orientation. Leg rotation speeds and rates of leg compression or extension can be found by differentiating sensor output. Recently it was shown that using low-cost state of the art sensors, it is possible to obtain good measurements of pitch and pitch velocity [13].

To give an overview of the control method, it is useful to follow the robot through the execution of one motion cycle, starting with liftoff, when the robot enters the flight phase. At liftoff the three control inputs are computed, based on the robot state. Once the inputs are known, the individual touchdown angles are known, from $\gamma_{sum,td}$, $\gamma_{dif,td}$, so the legs are positioned in flight. The leg positioning is accomplished using a simple PD control. When the stance phase begins, and given a transmission efficiency of η_a, the hip actuators are commanded to apply a constant torque τ_a, such that the applied torque is equal to the control input τ:

$$\tau_a = \tau / \eta_a \qquad (28)$$

At liftoff, at the end of stance, the cycle repeats.

V. Results

The control approach is evaluated for the real-world problem, using simulations of a detailed planar robot model, referred to as the test model, using the Working Model 2D software, see Fig. 7b. Simulations with adequate modeling have been shown to predict real quadruped motion [9].

The test model includes both robot and actuator modeling. The robot has body mass m_b =16 kg, leg spring constant k = 7000 N/m, body inertia I =1 kg·m^2, leg viscous friction b =15 N·s/m and leg rest length L =0.32 m. Half the hip spacing is d =0.25 m, and the dimensionless inertia is equal to $j = I/m_b d^2$ =1. The test model simulated also includes non-trivial leg mass, modeling of plastic foot-ground collisions, a DC motor model for the hip actuators, and a Coulomb foot-ground friction model allowing realistic foot slip. The DC motors are from Maxon Motors [10], of 60 W power, with nominal voltage 24 V, and torque constant 0.0259 N·m/A. Each motor weighs under 0.24 kg and the gear ratio is 50.

Initially, the response to height control is tested. The robot response is shown in Fig. 4, and the desired height trajectory in Fig. 4b, together with the apex height attained.

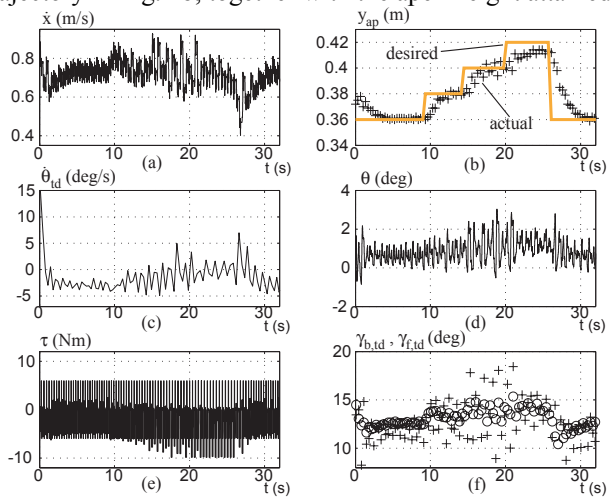

Fig. 4 Robot response to height control, at a speed of 0.8 m/s, (a) forward speed, (b) height at apex and desired in orange, (c) pitch velocity at touchdown, (d) body pitch, (e) sum of applied torque on both back legs, (f) back and front leg touchdown angles.

The maximum error in steady-state is less than 1cm, and then only for the largest apex height, which gives a ground clearance of 10cm. This is where fluctuations in the forward speed appear, see Fig. 4a. It can be seen that the torques applied by the actuators, in Fig. 4e, are completely realistic.

Secondly, results from following a desired forward speed trajectory are shown in Fig. 5. The trajectory is shown in Fig. 5a with a solid line, together with the actual speed, for a range of 0.6 to 1.5 m/s. The pitching motion is not shown for space economy, but it resembles the response in Fig. 4. The desired apex height of 36 cm is maintained, see Fig. 5b.

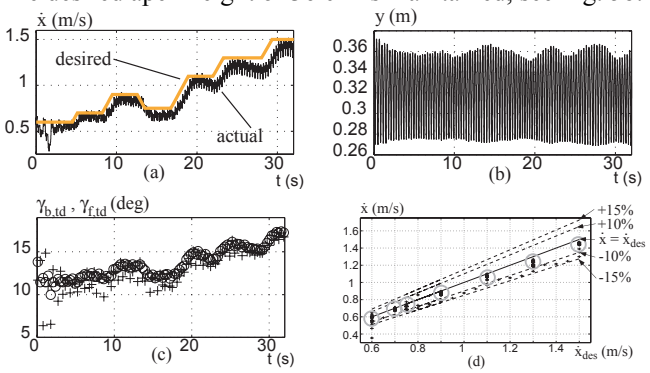

Fig. 5 Robot response to speed control, for a constant apex height of h=0.36 m, (a) forward speed and desired in orange, (b) CoM height, (c) leg touchdown angles. (d) Actual forward speed versus desired value (with crosses). The solid line represents zero error, while dashed lines show deviations of 10% and 15%. Gray circles indicate steady-state motion.

The forward speed of the robot at each flight apex is plotted versus the desired speed, in Fig. 5d. Although overall errors of up to about 15% are observed, this also includes transient states of motion. The size of the errors can

be verified by observing the forward speed in Fig. 5a. The gray circles indicate the steady-state motions, where it can be seen that errors are limited to less than 10%.

The controller maintains a pronking gait, as can be seen by the almost total absence of the pitching motion in Figs. 4d, 4c. Further, in Figs. 4f, 5c, the leg touchdown angles used are realistic. It is also interesting to portray a small time window of the motion, as in Fig. 6. In Fig. 6a, the velocity of a robot foot relative to the ground is shown and the slip of the foot is visible as it touches the ground, due to the ground-foot friction model. Also, Fig. 6b depicts a detail of the actuator power. Because the applied torque during stance has been chosen to be constant, see (16), there is no negative actuator work during stance. This is interpreted as the control working in coordination with the natural dynamics, pumping only the required energy in to the system.

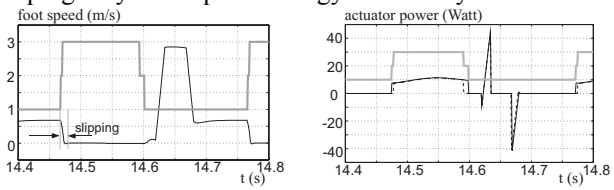

(a) (b)

Fig. 6 Response detail. (a) Foot slipping due to friction model, (b) actuator power for the back (solid) and front (dashed) motor. In both plots, the gray line denotes stance with its high value, and flight with its low value.

Now the case of the robot carrying a load is studied. The load is known, and is two loads of 2 kg placed at 11 cm each side of the body CoM, preserving mass symmetricity but changing total robot mass and inertia. The dimensionless inertia j is now 0.85, so the robot does not strictly belong to the class studied. Following the same speed trajectory as in Fig. 5, Fig. 7a shows good behavior all the way up to 1.3 m/s. Pitching was a little increased, but the 15% deviation in the dimensionless inertia did not result in control failure.

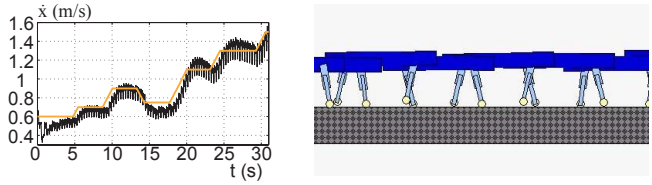

(a) (b)

Fig. 7 (a) Forward speed of robot with j=0.85. (b) Working Model 2D snapshots of running at 1.1 m/s.

A further interesting case is when the robot is made to carry asymmetric loads. For example, let two loads again be placed at 11 cm each side of the body CoM, except this time the loads are unequal, with masses of 1.5 kg and 2.5 kg. With this asymmetrical mass distribution the same speed trajectory as that used for Fig. 5 is applied. Despite the asymmetry, the control works well up to speeds of 1.1 m/s. However, if the asymmetry is increased by placing loads of 1kg, 3kg instead, the controller eventually fails.

The robot is also tested in the case of modeling error. Specifically, the robot parameters m_b, m_l, b, k, were all increased by 10% compared to the values used by the controller. In practice, error in parameter estimation will probably be smaller. Despite this, the robot followed the desired speed trajectory used for Fig. 5, up to speeds of 1.1 m/s, while pitching varied between -1 deg and 2 deg.

Finally, simulations in 3D were also performed using the ADAMS 3D simulation package. The controller response is similar to the Working Model 2D simulations. This result is expected, as the pronking gait studied here is symmetric with respect to the plane of forward motion.

CONCLUSIONS

In this work it has been shown how it is possible to control both the forward speed and height of a running quadruped, while retaining minimum pitching, using one actuator per leg. The control has been designed based on an insight of the robot dynamics and an unveiling of the effect of the leg touchdown angles. Extensive simulations showed the control to perform well, achieving high-speed running with almost no pitching. Negative actuator work was absent during stance, which reduced consumed energy by attracting the robot to the desired gait without working against the natural dynamics. This indicates that this work could contribute to designing lighter and more autonomous robots, as smaller actuators and power supplies could be used.

REFERENCES

[1] M. H. Raibert, "Legged robots that balance," *MIT Press*, Cambridge, MA, 1986.

[2] Z. Zhang, Y. Fukuoka and H. Kimura, "Adaptive running of a quadruped robot using delayed feedback control," *Proc. 2005 IEEE Int. Conf. on Robotics and Automation*, pp. 3750-3755, 2005.

[3] W. Marhefka, D. E. Orin, J. P. Schmiedeler and K. J. Waldron, "Intelligent control of quadruped gallops," *IEEE/ASME Transactions On Mechatronics*, Vol. 8, No. 4, pp. 446-456, 2003.

[4] Y. Fukuoka, H. Kimura and A. H. Cohen, "Adaptive dynamic walking of a quadruped robot on irregular terrain based on biological concepts," *The Int. Journal of Robotics Research*, Vol. 22, No. 3-4, pp. 187-202, 2003.

[5] S. Talebi, I. Poulakakis, E. Papadopoulos and M. Buehler, "Quadruped robot running with a bounding gait," *Proc. 7th Int. Symp. on Experimental Robotic (ISER'00)*, Honolulu, HI, pp.281-289, 2000.

[6] D. Papadopoulos and M. Buehler, "Stable running in a quadruped robot with compliant legs," *Proc. 2000 IEEE Int. Conf. Robotics and Automation*, San Francisco, CA, pp. 444-449, April 2000.

[7] M. Lasa and M. Buehler, "Dynamic compliant quadruped walking," *Proc. 2001 IEEE Int. Conf. on Robotics and Automation*, pp. 3153-3158, 2001.

[8] Murphy K. N. and Raibert M. H., "Trotting and Bounding in a Planar Two-legged Model," *5th Symp. on Theory and Practice of Robots and Manipulators*, A. Morecki, G. Bianchi, K. Kedzior (eds), MIT Press, Cambridge MA, pp. 411-420, 1984.

[9] I. Poulakakis, J. A. Smith and M. Buehler, "Modeling and experiments of untethered quadrupedal running with a bounding gait: the scout II robot," *The Int. Journal of Robotics Research*, Vol. 24, No. 4, pp. 239-256, 2005.

[10] Maxon Motor AG, www.maxonmotor.com.

[11] N. Cherouvim and E. Papadopoulos, "Single Actuator Control Analysis of a Planar Hopping Robot," *Proc. Robotics: Science and Systems 2005,* MIT, Cambridge, MA, 2005.

[12] M. D. Berkemeier, "Approximate Return Maps for Quadrupedal Running," *Proc. 1997 IEEE Int. Conf. on Robotics and Automation*, pp. 805-810, 1997.

[13] J. Leavitt, A. Sideris and J. E. Bubrow, "High Bandwidth Tilt Measurement Using Low-Cost Sensors," IEEE/ASME Transactions on Mechatronics, vol. 11, no. 3, pp. 320-327, 2006.